Saudi Journal of Biological Sciences 29 (2022) 894–904

Contents lists available at ScienceDirect

Saudi Journal of Biological Sciences

journal homepage: www.sciencedirect.com

Original article

# Antioxidant, antibacterial, and catalytic performance of biosynthesized silver nanoparticles of *Rhus javanica*, *Rumex hastatus*, and *Callistemon viminalis*

Wajheeba Khan [a], Naeem Khan [b], Nargis Jamila [a,*], Rehana Masood [c], Aaliya Minhaz [a], Farhat Amin [d], Amir Atlas [e], Umar Nishan [b]

[a] Department of Chemistry, Shaheed Benazir Bhutto Women University, Peshawar 25000, Khyber Pakhtunkhwa, Pakistan
[b] Department of Chemistry, Kohat University of Science and Technology, Kohat 26000, Khyber Pakhtunkhwa, Pakistan
[c] Department of Biochemistry, Shaheed Benazir Bhutto Women University, Peshawar 25000, Khyber Pakhtunkhwa, Pakistan
[d] Department of Bioinformatics, Shaheed Benazir Bhutto Women University, Peshawar 25000, Khyber Pakhtunkhwa, Pakistan
[e] Institute of Basic Medical Sciences, Khyber Medical University, Peshawar 25000, Khyber Pakhtunkhwa, Pakistan

ARTICLE INFO

*Article history:*
Received 25 August 2021
Revised 22 September 2021
Accepted 4 October 2021
Available online 11 October 2021

*Keyword:*
*Rhus javanica*
*Rumex hastatus*
*Callistemon viminalis*
AgNPs
Antibacterial
Rhodamine B

ABSTRACT

*Rhus javanica* (Anacardiaceae) containing abundant glucopyranosidal constituents, is traditionally used to treat gastric and duodenal ulcer, dysentery, and diarrhea. *Rumex hastatus* (Polygonaceae) widely distributed in Pakistan, has traditional importance in treating wound healing, jaundice, rheumatism, and skin diseases. *Callistemon viminalis* (Myrtaceae), a rich source of essential oils, saponins, triterpenoids, phloroglucinols, and flavonoids is used in industries, perfumes, nutrition, and cosmetics. Taking the importance of the subject plants, this study is designed to synthesize silver nanoparticles via aqueous extracts of *R. javanica* (RJAgNPs), *R. hastatus* (RHAgNPs), and *C. viminalis* (CVAgNPs). Synthesis, surface, and sizes of silver nanoparticles (AgNPs) were confirmed using spectroscopic techniques including ultraviolet–visible (UV–Vis), Fourier transform-infrared (FT-IR), and scanning electron microscopy (SEM). AgNPs were produced in ratios 1:15, 1:16, and 1:9 and inferred via appearance of a sharp surface plasmon resonance (SPR) absorption peak (400–435 nm), which represented well-defined, stable, and spherical AgNPs. From SEM analysis, the sizes of RJAgNPs, RHAgNPs, and CVAgNPs were found to be 67 nm, 61 nm, and 55 nm, respectively. The synthesized AgNPs exhibited potential free radical scavenging, antibacterial, and catalytic properties in degradation of dyes including Congo red, methylene blue, methyl orange, rhodamine B, *ortho* and *para*-nitrophenols, and several food colours. Hence, the subject AgNPs in the current study might display promising role in drug development and remediation of environmental/industrial effluents.



## 1. Introduction

Nanoparticles (NPs) have wide range of application in biomedical sciences, biomechanics, medicine, and environmental remediation. Metal nanoparticles (MNPs) have gained high importance due to the vast application in photonics, optoelectronics, biological tagging catalysis, drug delivery, and biomedical devices (Jain & Mehata, 2017; Yu et al., 2020; Sahu et al., 2021). Noble metals (silver, gold and platinum) NPs have been widely used in a variety of domestic products such as filters, nanocomposites, toothpastes, shoes, and cleansing and personal care products (ElMitwalli et al., 2020; Jadoun et al., 2021; Yang et al., 2021). These NPs can be synthesized by various physical and chemical methods. However, the subject methods are considered eco-unfriendly due to the use of toxic organic solvents and reducing agents. Therefore, the biogenic NPs utilizing plants, algae, and microorganisms put a route of green synthesis due to reduced environmental impacts (Hassan et al., 2021; Soni et al., 2021).

Among MNPs, silver nanoparticles (AgNPs) are of specific medicinal interest because of antimicrobial properties of Ag metal. These

* Corresponding author.
*E-mail address:* nargisjamila@sbbwu.edu.pk (N. Jamila).
Peer review under responsibility of King Saud University.

Production and hosting by Elsevier

https://doi.org/10.1016/j.sjbs.2021.10.016
1319-562X/

have been potentially used as antimicrobial agent against a wide range of bacteria and fungi in wound dressing, medical implants coatings, ointments, lining of food containers, and cancer therapy (Farhadi et al., 2017). In addition, MNPs, due to high surface reactivity, large surface area, strong adsorption capacity, and high catalytic efficiency, have been reported to detect dyes/pollutants (Nguyen et al., 2021). Synthetic organic dyes are extensively used in textile, cosmetics, plastic, food, medicinal drugs, and several other industries. These industries release a large amount of various excessive unfixed dyes such as azo (Congo red, methyl orange), and cationic (Rhodamine B), which could be toxic to ecosystem and human health. Azo dyes on reductive cleavage lead to the formation of carcinogenic amines. Therefore, upon adsorption/dissolution by soil or water, these dyes may cause destruction of flora, microorganisms, and aquatic biota, which damage the environment and agricultural productivity (Jadhav et al., 2019). Therefore, researchers have interest to develop new technologies for entrapping the released excessive dyes coming from various industries.

Plants are the natural "chemical factories" of large number of metabolites having oxidizing and reducing capacity to boost up safe and stable NPs synthesis (Marslin et al., 2018; Wu et al., 2018; Nobahar et al., 2021). Therefore, nowadays, the area of MNPs synthesis using plant/herbs is an increasing focus of attention. Generally, when aqueous solution of a relevant salt is mixed with the plant aqueous extract, a reaction occurs and completes within few minutes at ambient temperature. In the current study, *Rhus javanica*, *Callistemon viminalis*, and *Rumex hastatus* collected from different areas of Pakistan were selected for AgNPs synthesis.

*Rhus javanica* (Anacardiaceae) given as Fig. 1a is traditionally used to treat dysentery, diarrhea, and gastric and duodenal ulcer (Kim et al., 2003). This plant is a rich source of flavonoids and the corresponding glycosides, which inhibit the multiplication of tobacco mosaic virus (Ouyang et al., 2007). *Rumex hastatus* (Polygonaceae) given as Fig. 1b is used as traditional medicine to treat diarrhea, dysentery, wound healing, jaundice, rheumatism, and skin diseases. Due to the abundance of essential oil, this plant is also used as a flavouring agent. It contains flavonoids, phenolics, tannins, saponins, which possess significant antioxidant, antidiarrheal, anti-inflammatory, antimicrobial, and cytotoxic activities (Makkar et al., 1993; Liang et al., 2010; Sahreen et al., 2014: Ahmad et al., 2016a; Ahmad et al., 2016b; Mishra et al., 2018). *Callistemon viminalis* (Myrtaceae) given as Fig. 1c is a rich source of antioxidative and antimicrobial essential oils, saponins, alkaloids, triterpenoids, phloroglucinols, and flavonoids, which perform important role in pharmaceutical industries, perfumes, nutrition, and cosmetics (Oyedeji et al., 2009; Salem et al., 2013; Liu et al., 2016; Salem et al., 2017; Liu et al., 2018).

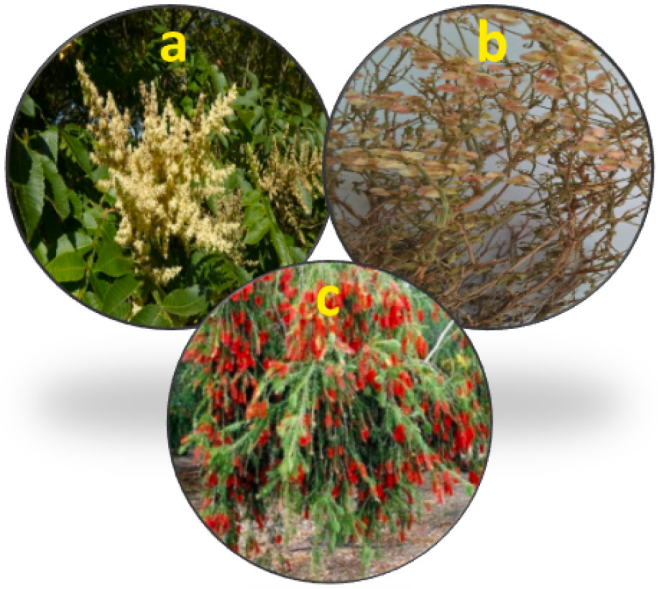


**Fig. 1.** (a) *Rhus javanica*, (b) *Rumex hastatus*, and (c) *Callistemon viminalis* plants used in this study for AgNPs synthesis.

Taking the medicinal importance and lack of nanostructural study on subject plants, and antimicrobial and catalytic potential of AgNPs into account, the current study was aimed to synthesize AgNPs, and determine the antibacterial (*Staphylococcus aureus*, *Escherichia coli*), antioxidant (2,2-diphenyl-1-picrylhydrazyl; DPPH, 2′-azino-bis-3-ethyl benzthiazoline-6-sulphonic acid; ABTS), and catalytic potential in dyes and food colours degradation. The dyes and food colours selected for catalytic activity evaluation were methylene blue (MB), methyl orange (MO), Congo red (CR), Rhodamine B (RdB), ortho and *para*-nitrophenols (ONP, PNP), zarda yellow (ZY), bright red (BR), and deep green. Abbreviations used in this study are enlisted as Table 1.

## 2. Materials and methods

### 2.1. Samples collection

Fresh bark of *R. javanica* was collected from District Barawal (Dir Upper, Khyber Pakhtunkhwa, Pakistan) in May 2019. *R. hastatus* whole plant was collected from Tirah (Khyber Agency, Khyber Pakhtunkhwa, Pakistan) in September 2019. The fresh flowers of *C. viminalis* were collected from the garden of Pakistan Locomotive Factory Risalpur (Khyber Pakhtunkhwa, Pakistan) in May 2019. The plants were identified by Dr. Nadeem Ahmad, Department of Botany, University of Peshawar (Pakistan). Before use, the samples were cleaned to remove all the dust, dried, powdered, and then stored for further use.

### 2.2. Chemicals/reagents and instrumentation

Deionized water was used as a solvent for extraction. Chemicals including $AgNO_3$, DPPH, ABTS, sodium borohydride ($NaBH_4$), CR, MB, RdB, MO, ONP, PNP, gallic acid, streptomycin, vancomycin, and bacterial strains (*S. aureus* and *E. coli*) were purchased from Merck and Sigma-Aldrich (Germany). Food dyes (ZY, DG, and BR) were obtained from local super market. Agar media for antibacterial activity was procured from Oxoid (England). To confirm synthesis of AgNPs, and evaluation of antioxidant activity, a UV-1800 double beam spectrophotometer (Shimadzu, Japan) was used. Functional groups of the phytoconstituents/reducing agents present in the extracts were determined using FT-IR spectrometer (Bruker). Sizes of the synthesized AgNPs were determined by field

**Table 1**
Nomenclature of the materials used.

| Abbreviations | Full Name |
|---|---|
| AgNPs | Silver nanoparticles |
| BR | Bright red |
| CR | Congo red |
| CVAE | *Callistemon viminalis* aqueous extract |
| CVAgNPs | *C. viminalis* silver nanoparticles |
| DG | Deep green |
| MB | Methylene blue |
| MO | Methyl orange |
| RdB | Rhodamine B |
| ONP | *ortho*-nitrophenol |
| PNP | *para*-nitrophenol |
| RHAE | *Rumex hastatus* aqueous extract |
| RJAE | *Rhus javanica* aqueous extract |
| RHAgNPs | *R. hastatus* silver nanoparticles |
| RJAgNPs | *R. javanica* silver nanoparticles |
| ZY | Zarda yellow |

emission-scanning electron microscope, FE-SEM (S-4800, Hitachi, Japan) operated at an accelerating voltage of 15 kV, magnification x2.0 k, working distance 7.7 mm, and high lens mode.

### 2.3. Preparation of plants' aqueous extracts

Fresh *R. javanica* (bark), *R. hastatus* (aerial part), and *C. viminalis* (flowers) were shade dried. The dried samples were crushed in a grinder into fine powder. A 25 g of the powdered samples were mixed with deionized water (250 mL). The mixture was stirred on a magnetic stirrer at 500 rpm and 60 °C for 2 h to obtain aqueous extracts of *R. javanica* (RJAE), *R. hastatus* (RHAE), and *C. viminalis* (CVAE). The obtained extracts were filtered through common filter paper, followed by 0.45 μm Millipore filter, and stored in a refrigerator until next use.

### 2.4. Synthesis and characterization of AgNPs

NPs were biosynthesized via mixing silver nitrate ($AgNO_3$) salt solution with aqueous extracts of the subject plants in various ratios. The reaction mixtures were analyzed at intervals of 0 min to 6 h, and different conditions such as heating and stirring (50 °C, 500 rpm), stirring, sunlight, and incubation (ambient temperature). The colour of the mixtures was noticed at zero to 30 min. Change in colour from yellow to dark brown indicated the reduction process and correspondingly the synthesis of NPs (Fig. S1, supplementary material). The corresponding AgNPs were confirmed by measuring UV–Vis spectra where the appearance of surface plasmon resonance (SPR) band in the range of 400–435 nm is attributed to AgNPs formation. The corresponding AgNPs solutions were centrifuged at a speed of 4000 rpm × g. An obtained

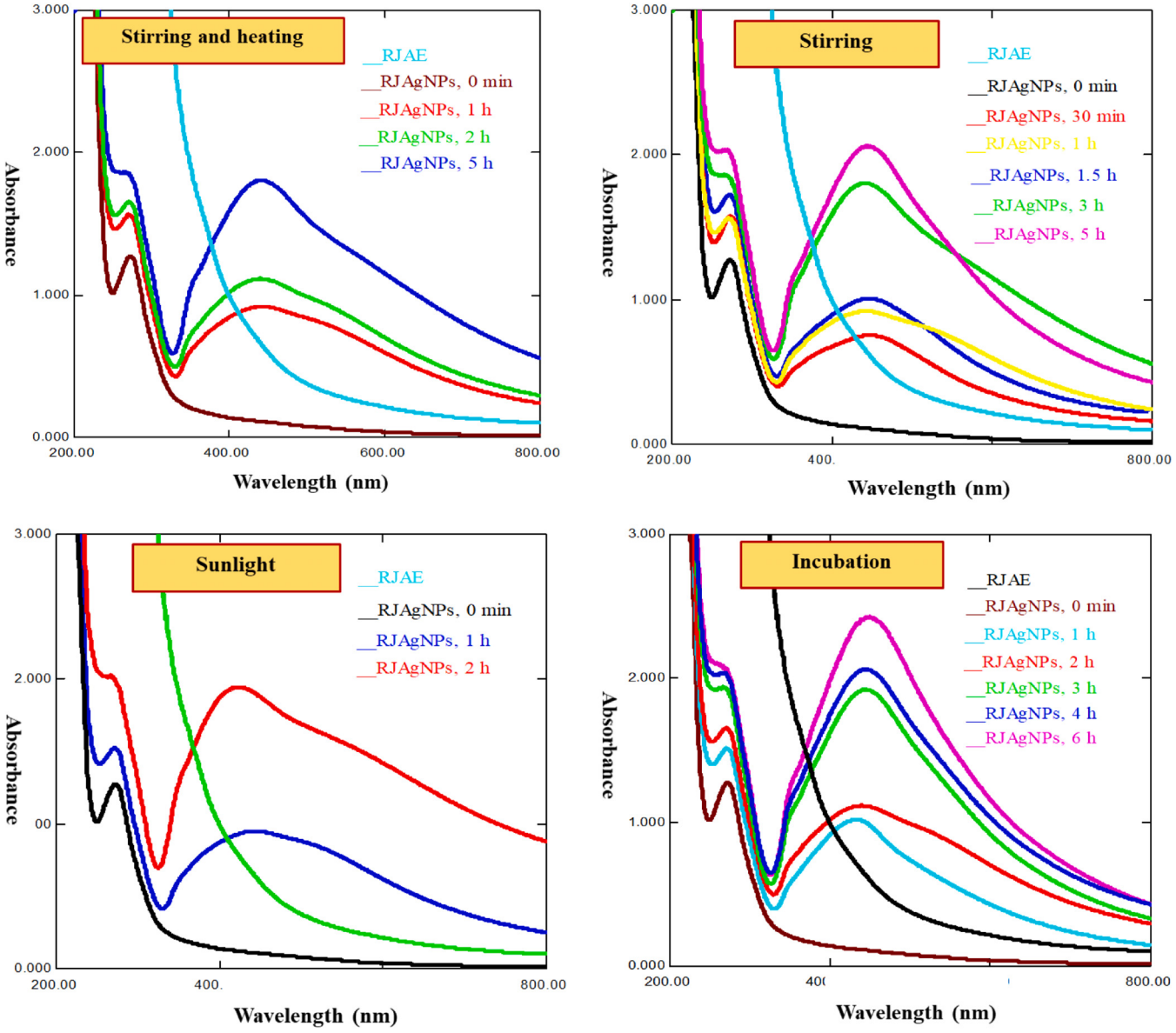


**Fig. 2.** UV–Vis spectral graphs of RJAgNPs synthesized in 1:15 ratio at all four conditions.

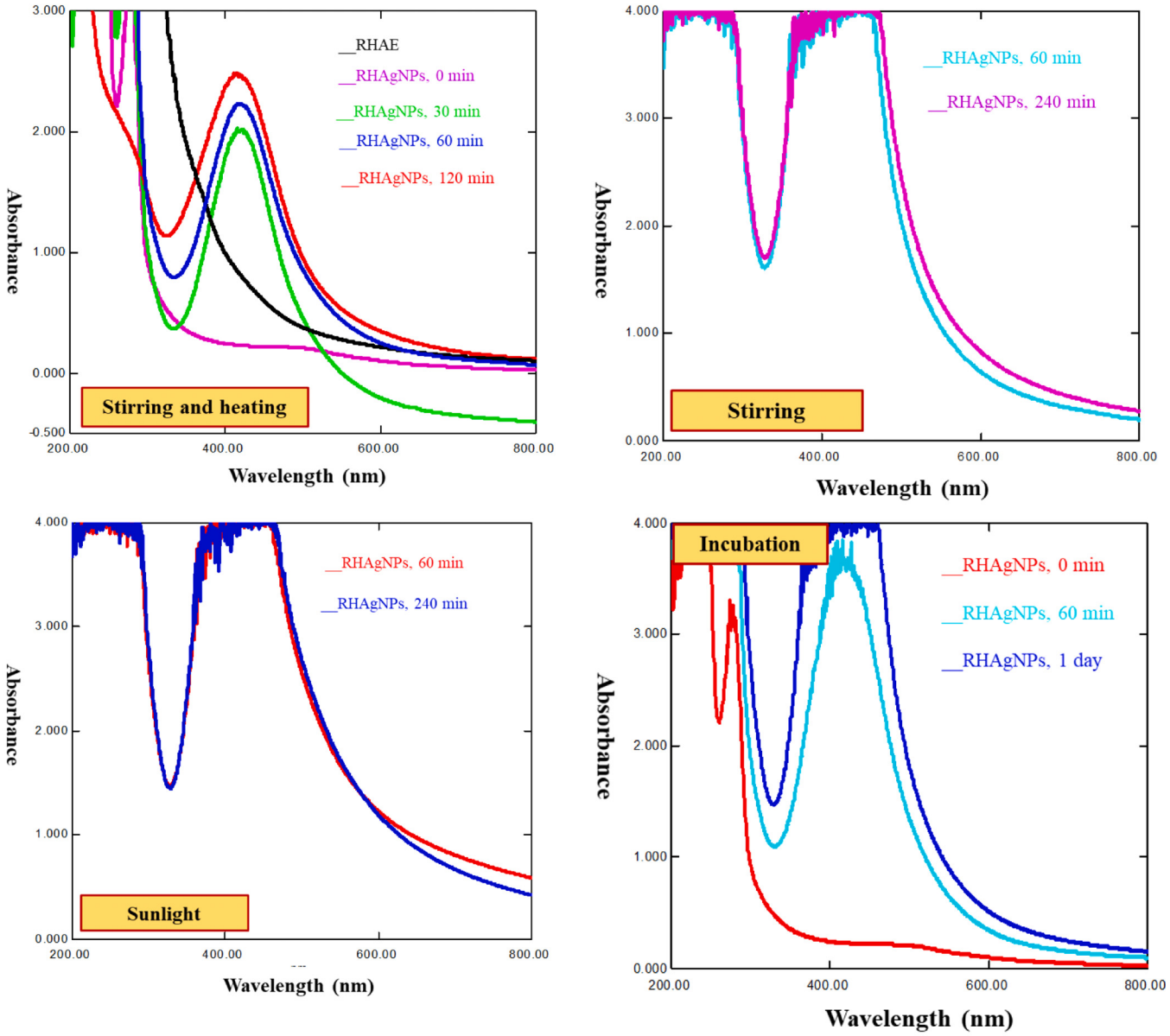


**Fig. 3.** UV–Vis spectral graphs of RHAgNPs synthesized in 1:15 ratio at all four conditions.

solid product was vacuum dried and stored for further analysis/characterization by FT-IR and SEM techniques, antioxidant, antibacterial, and catalytic potential in dyes degradation.

### 2.5. Antioxidant and antibacterial activities of AgNPs

For determining antioxidant activity by DPPH and ABTS assay, and antibacterial potential by disc diffusion and minimum inhibitory concentration methods, first, the stock solutions (1000 μg/mL) of the corresponding AgNPs were prepared. Then, the working solutions were prepared via two-fold dilution. For analysis, the established protocols (Jamila et al., 2014; Jamila et al., 2020) were respectively followed for antioxidant and antibacterial assays.

### 2.6. Catalytic activity of AgNPs in dyes degradation/reduction

For this activity, the published protocols (Jamila et al., 2020; Jamila et al., 2021) were followed. Briefly, a reaction mixture was prepared by adding $NaBH_4$ (0.1 mM, 0.5 mL) to 2.5 mL of dyes/food colours. Then, the mixture was analyzed via UV–Vis spectrophotometer. After that, AgNPs (5 mg) were added to the reaction mixture and spectral analysis was conducted. The %degradation/reduction indicated the dyes degradation and calculated via Eq. (1) using the absorbance data obtained at different intervals (Khan et al., 2019).

$$\% \text{ degradation/reduction} = (1 - A_t/A_0) \times 100 \quad (1)$$

## 3. Results

### 3.1. Synthesis and characterization of AgNPs

In the current research study, the AgNPs were synthesized in different ratios (starting from 1:1) at stirring, heating & stirring, incubation, and in the sunlight. The AgNPs production was primarily detected via colourimetric changes from yellow to reddish brown, and, then by observing SPR peak in UV–Vis spectroscopic analysis. Among the AgNPs, well-stable RJAgNPs were formed via

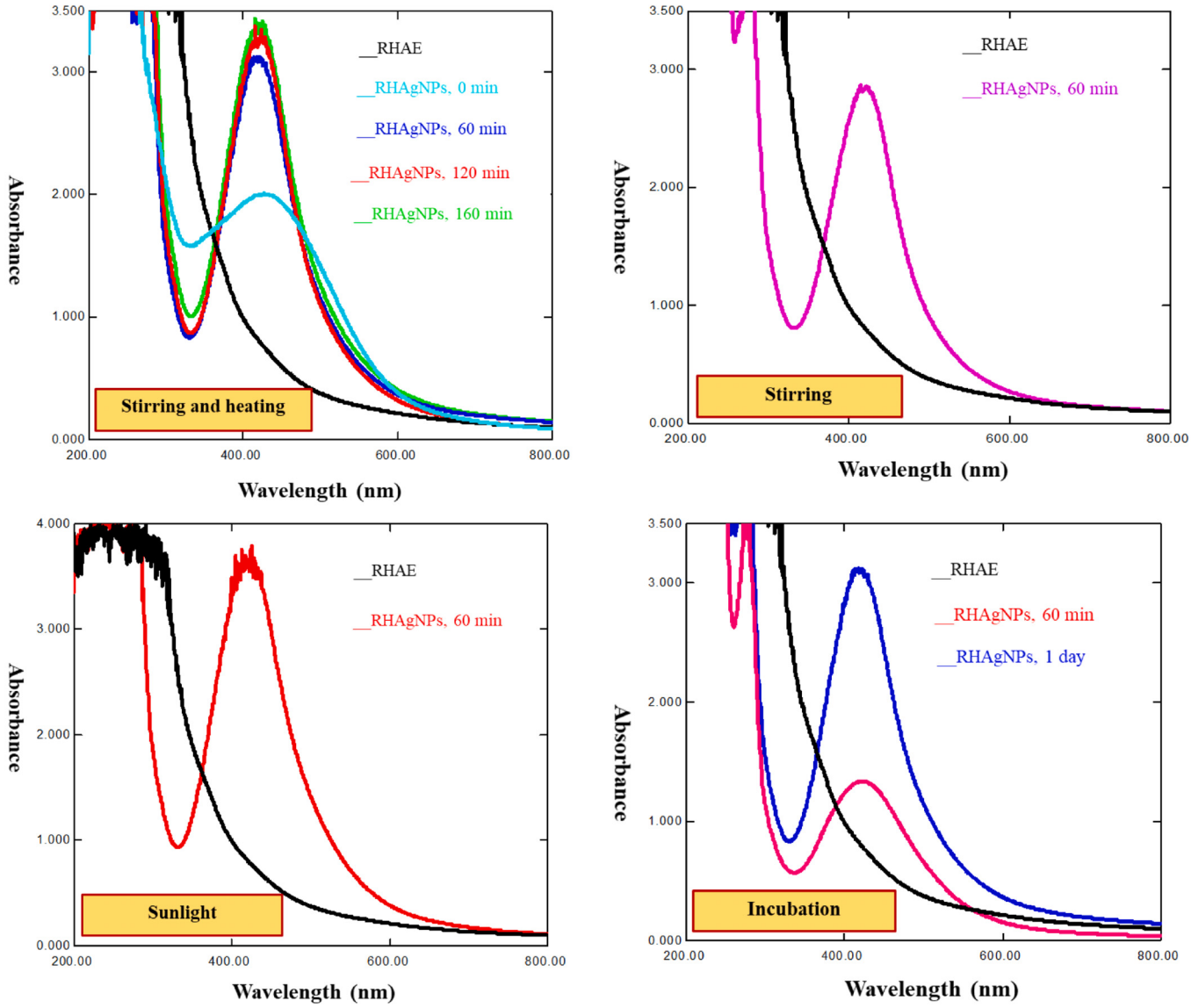


**Fig. 4.** UV–Vis spectral graphs of RHAgNPs synthesized in 1:16 ratio at all four conditions.

a mixture of 1:15 of aqueous extract and the salt, respectively, under stirring, and incubation, where the UV–Vis spectra exhibited a sharp SPR absorption band at 430 nm in a time range of 3–6 h (Fig. 2). However, under heating & stirring, and sunlight, unstable AgNPs exhibiting broad SPR peaks, were produced. Regarding RHAgNPs, these were formed in ratios of 1:1 to 1: 14 up to 3 h. However, proceeding to 1:15 to 1:17 ratios, the most significant RHAgNPs were produced (Figs. 3-5) under all the four conditions showing maximum absorption at 427 nm, which represents the spherical shaped AgNPs formation. CVAgNPs synthesized in ratios starting from 1:1, only a ratio 1:9 afforded significant AgNPs in sunlight as indicated by a sharp SPR band at 431 nm (Fig. 6). However, applying the conditions of stirring & heating, stirring, and incubation, no significant CVAgNPs were formed.

Regarding the FT-IR analysis, spectra of the subject aqueous extracts displayed prominent absorption frequencies at 3500–3200 $cm^{-1}$ (O—H, hydroxyl) and 1750–1560 $cm^{-1}$ (C═O, carbonyl) (Fig. S2, supplementary material). However, in the FT-IR spectra of corresponding AgNPs (Fig. S2, supplementary material) exhibited reduced absorption frequencies of O—H group in RJAgNPs and CVAgNPs, whereas RHAgNPs have shown reduced O—H and C═O groups frequencies. In morphological characterization, the images and the particle size distribution graphs (Fig. 7) depict that polydispersed RJAgNPs (1:15), RHAgNPs (1:16), and CVAgNPs (1:9) have sizes of 67 nm, 61 nm, and 55 nm, respectively.

### 3.2. Antioxidant and antibacterial activities of AgNPs

The antioxidant activity assessed against DPPH and ABTS free radicals have shown that CVAgNPs have stronger *in vitro* antioxidant potential against DPPH and ABTS radicals, which exhibited the $IC_{50}$ values of 62.2 μg/mL and 52.1 μg/mL, respectively (Fig. 8). In antibacterial activity, the results (Table 2) exhibited that RJAgNPs is the most effective inhibitor to the subject strains showing inhibition zones of 19.0 mm and 10.0 mm, and $IC_{50}$ values; 62.5 μg/mL and 125 μg/mL for *S. aureus* and *E. coli*, respectively.

### 3.3. Catalytic activity of AgNPs in dyes degradation/reduction

In the current study, the catalytic property of the subject AgNPs as nanocatalysts for dyes degradation was determined, where the dyes were reduced using $NaBH_4$ in the presence as well as absence

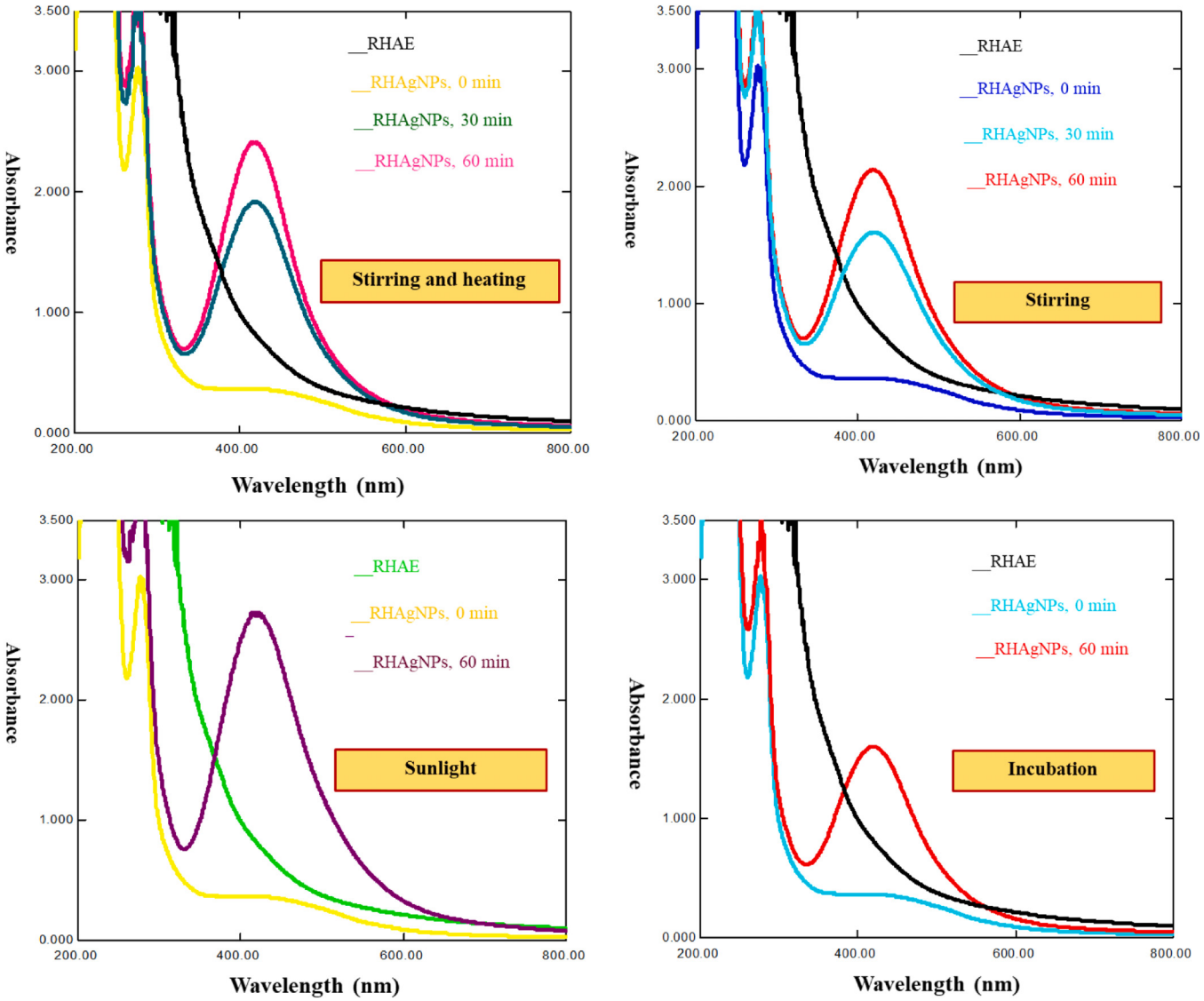


**Fig. 5.** UV–Vis spectral graphs of RHAgNPs synthesized in 1:17 ratio at all four conditions.

of the subject AgNPs. From the results, it was found that when the reaction is carried out in the absence of AgNPs, a very small change in the mixture colour, and the decrease in the absorption maxima is observed even after 30 min. However, upon the addition of AgNPs to the reaction mixture, the color of dyes solutions became faint (Fig. S3, supplementary material) and dyes discoloration occurs within 5–10 min, which is proposed to be due to reduction reaction. For example, the blue colour of MB upon the addition of subject AgNPs disappeared due to its reduction to a colourless leucomethylene blue (LMB). Similarly, the degradation of MO can be highlighted in the UV–Vis spectra where, with the passage of time, a decrease in absorbance at $\lambda_{max}$ of 462 nm (for MO) and an increase in absorbance at $\lambda_{max}$ of 239 nm (for amine group from degraded MO) was observed (Fig. 9). In determining the %dyes reduction calculated using equation (1), varied range of %removal was obtained as; CR (80 to 85%), MB (70 to 80%), RdB (65 to 70%), MO (80 to 83%), PNP (75 to 80%), ONP (75 to 80%), BR (78 to 83%), DG (78 to 82%), and ZY (78 to 82%) at a contact time of 120 min. After that, the rate of reaction and the catalytic efficiency almost stopped.

## 4. Discussion

Plant extracts contain different content and combinations of bioactive secondary metabolites/polyphenolics. These polyphenolics containing several hydroxyl groups may act as reducing agents in NPs synthesis (Erci et al., 2018). It is a well-known fact that the brown color of AgNPs solution is because of the excited state of SPR vibrations (400–450 nm) from the $Ag^{+}$ reduction to $Ag^{0}$. Intensity of brown color and the SPR band increased with the passage of time (0 min to 5 h) because of the increased excitation of SPR effect, reduction of $Ag^{+}$ ions, and production of high content of AgNPs. The UV–Vis technique in a range of 400–450 nm is a commonly used in characterizing AgNPs having sizes in the range of 1 to 100 nm. SPR patterns and characteristics of MNPs strongly depend on particle size, stabilizing molecules, and the dielectric constant of medium. In the UV–Vis spectra of the subject AgNPs, not absorbance at 335 and 560 nm were found, indicating the dispersed AgNPs formation and ultimately no aggregation process.

The chemical composition and functional groups of the phytoconstituents of the subject plant extracts, and their involvement

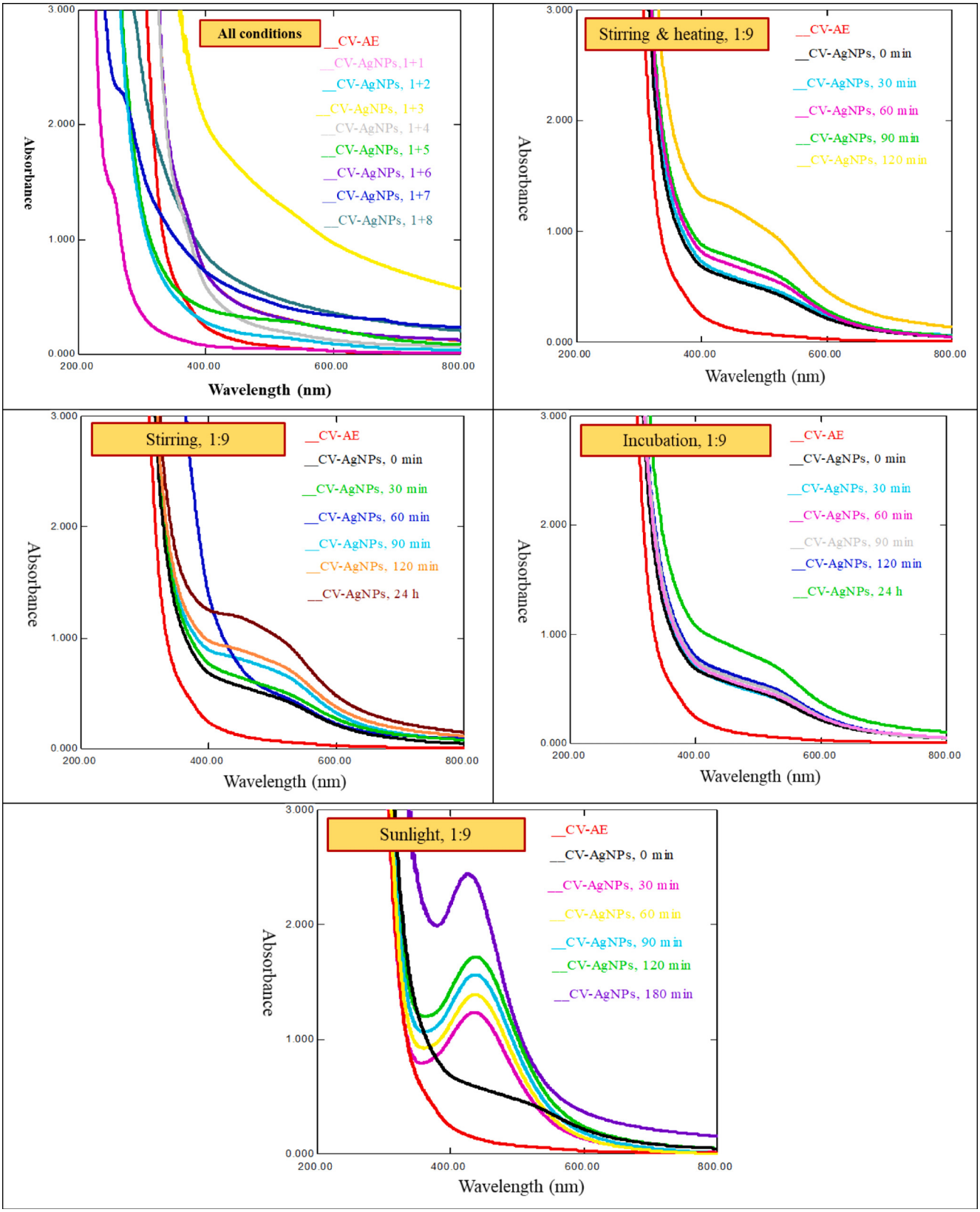


**Fig. 6.** UV–Vis spectral graphs of CVAgNPs synthesized in 1:1 to 1:9 ratios at all four conditions.

in the corresponding AgNPs synthesis were analyzed via FT-IR spectroscopy, which characterizes the carbonyls, hydroxyls, carboxylic, amide, and any other functional groups, functioning as reducing agents and attached to the AgNPs surfaces (Kamnev et al., 2021). The absorption frequencies exhibited at 3330 $cm^{-1}$ and 1700–1600 $cm^{-1}$ present in the FT-IR spectra of plant extracts

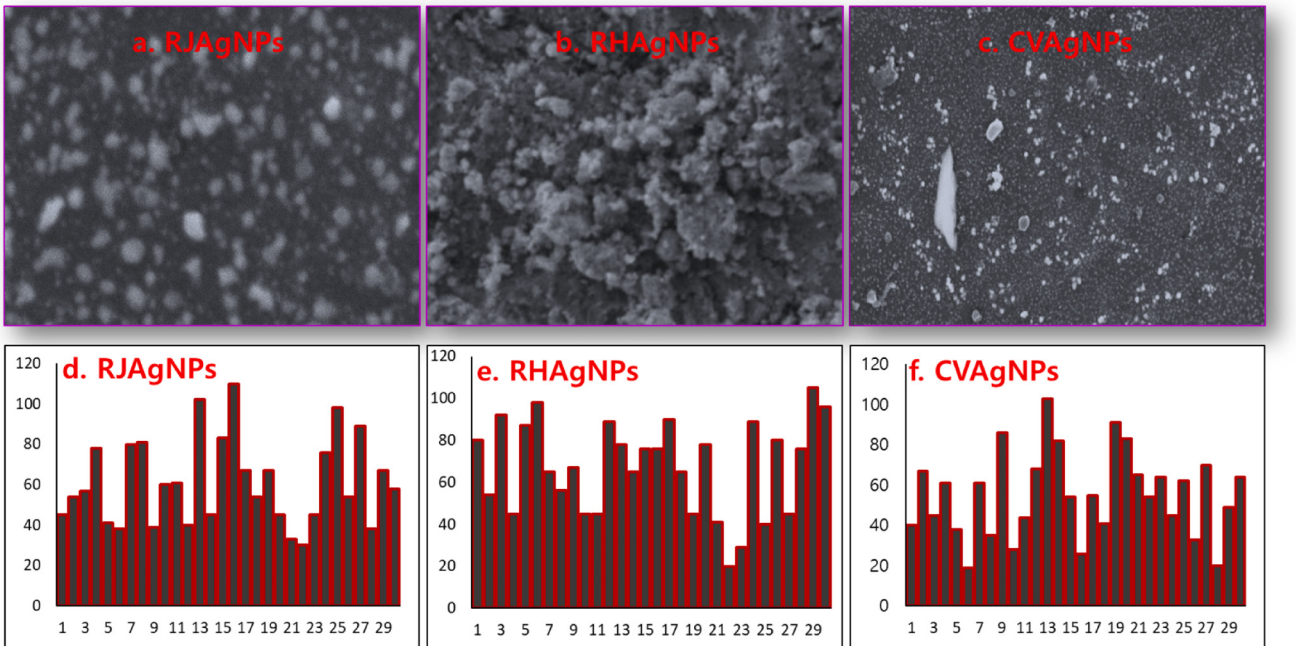


**Fig. 7.** SEM images (a-c) and the particle size distribution graphs (d-f) of the synthesized RJAgNPs, RHAgNPs, and CVAgNPs.

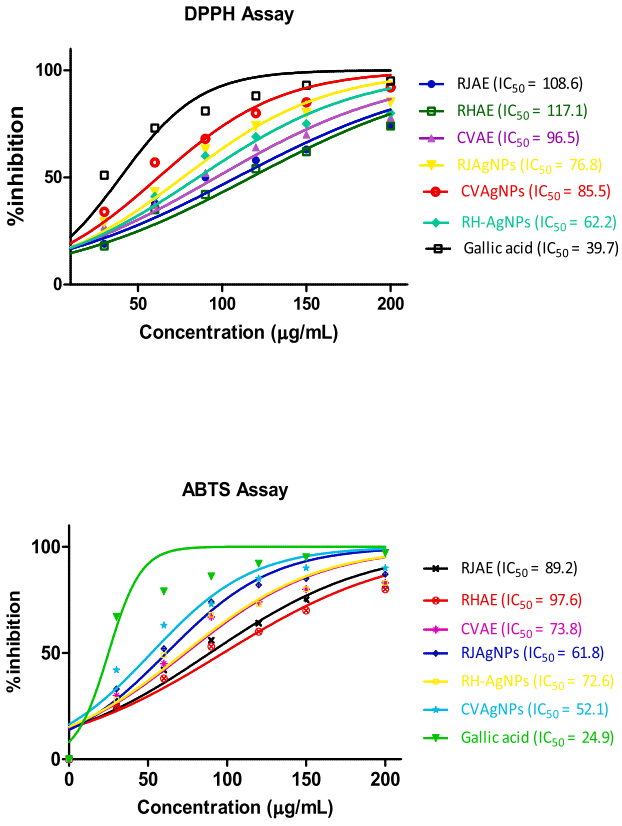


**Fig. 8.** Antioxidant activity (DPPH and ABTS assays) of RJAE, RHAE, CVAE, RJAgNPs, RHAgNPs, and CVAgNPs.

were attributed to the stretching vibration of —COOH and —NH (amino) groups. However, FT-IR spectra of the corresponding AgNPs displayed changes in the absorption frequencies for —COOH and —NH groups, which conclude the involvement of these functional groups in the AgNPs synthesis of the selected plants.

For antioxidant activity evaluation of the subject plant extracts and AgNPs, DPPH and ABTS free radicals assays were selected due to visual observation/colourimetric changes, efficiency, time-effective, and simple operating procedure. The antioxidant activity of phytoconstituents is supposed to be due to the number, location and bond dissociation energy of O—H group, and stability, resonance delocalization and steric hindrance of phytoconstituents. In addition, it was observed that compared to DPPH radical, the inhibition of ABTS radical by AgNPs was fast. Previous literature reported that the inhibition of ABTS radical depends only upon the number of O—H group irrespective of the position on the basic nucleus of antioxidative metabolites. However, DPPH inhibition is in close relation to the number as well as location of the O—H group (Jamila et al., 2014). The potent antioxidant activity of RJAgNPs might be due to its large surface area to volume ratio, which increases the chances of exposure to free radicals (Ezhilarasu et al., 2020). The selected plants for this study are rich sources of flavonoids, phenolics, tannins, saponins, alkaloids, and phloroglucinols. Therefore, the significant radical scavenging potential of the subject AgNPs suggests that the concentration of the polyphenolics on the surface of the NPs is present, and hence, inhibit the free radicals efficiently.

AgNPs due to their high surface-area-to-volume ratio exhibit significant antimicrobial activity against multidrug resistant (MR) bacteria, for example, *E. coli* and *Staphylococcus aureus* (Loo et al., 2018). Hence, in the current study, the subject AgNPs were tested against these bacterial strains. The bacterial inhibition mechanism of AgNPs is proposed to be due to a slow release of $Ag^{+}$ ions (oxidation) in or outside the cell, which affects the permeability of membranes of microbial cells, inactivate proteins, and interfere with the replication of DNA, which further disables the nuclear machinery of the cell (Lin et al., 2021). In this study, the significant antibacterial activity of the AgNPs might be attributed to the above stated mechanism.

Synthetic organic dyes are widely used in several industries such as textile, cosmetics, plastic, and food. The excessive unfixed dyes are released as effluents and could be toxic to human health, ecosystem, and aquatic biota, thus, damaging the environment and agricultural productivity (Jadhav et al., 2019). These dyes are there-

**Table 2**
Antibacterial activity of RJAE, RHAE, CVAE, RJAgNPs, RHAgNPs, and CVAgNPs by disc diffusion (DD) and minimum inhibitory concentration (MIC) assays.

| Samples | Disk diffusion (mm) | | Minimum inhibitory concentration method (μg/mL) | |
|---|---|---|---|---|
| | *S. aureus* | *E. coli* | *S. aureus* | *E. coli* |
| RJAE | 10.5 ± 1.0 $^{cd}$ | 7.0 ± 0.5$^{b}$ | 250$^{c}$ | 1000$^{e}$ |
| RHAE | 8.0 ± 0.5$^{a}$ | 6.0 ± 0.5$^{a}$ | 250$^{c}$ | 1000$^{e}$ |
| CVAE | 9.5 ± 1.0$^{b}$ | 7.0 ± 0.5$^{b}$ | 250$^{c}$ | 500$^{d}$ |
| RJAgNPs | 19.0 ± 1.5$^{f}$ | 10.0 ± 1.0$^{e}$ | 62.5$^{b}$ | 125$^{b}$ |
| RHAgNPs | 10.0 ± 1.0$^{bc}$ | 7.0 ± 0.5$^{b}$ | 250$^{c}$ | 500$^{d}$ |
| CVAgNPs | 15.0 ± 1.0$^{e}$ | 8.5 ± 1.0$^{d}$ | 62.5$^{b}$ | 250$^{c}$ |
| Vancomycin* | 19.5 ± 0.5 $^{fg}$ | 11.0 ± 0.5$^{f}$ | 31.5$^{a}$ | 125$^{b}$ |
| Streptomycin* | 20.5 ± .5$^{h}$ | 19.5 ± 0.5 $^{g}$ | 31.5$^{a}$ | 31.5$^{a}$ |

*Represents standard drugs.

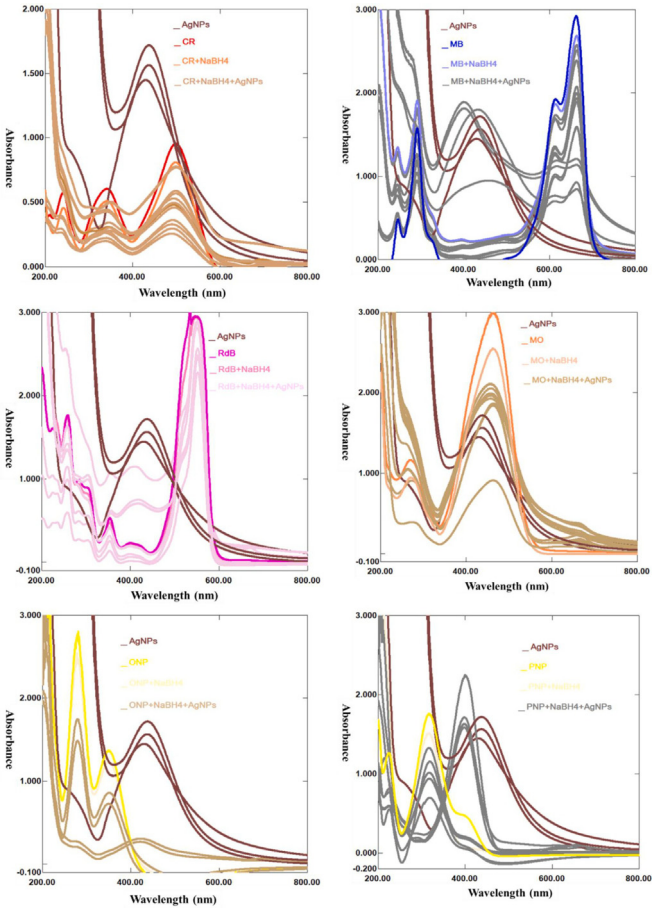


**Fig. 9.** UV–Vis spectral graphs of the catalytic potential of RJAgNPs, RHAgNPs, and CVAgNPs in dyes, nitrophenols, and food colours reduction.

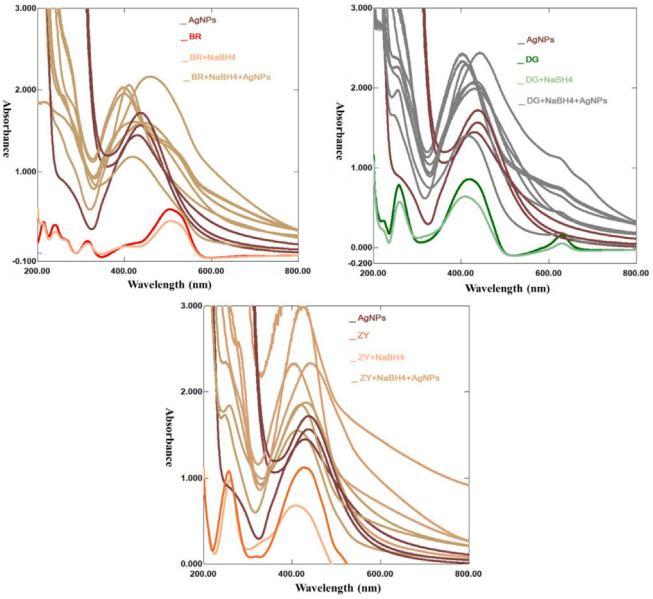


**Fig. 9** (*continued*)

fore necessary to remove from the environment. Recently, due to simplicity, cost effectiveness, efficiency, and mainly because of large surface area to volume ratios, bio-green MNPs are being given considerable attention as nanoadsorbents for dyes (Khan et al., 2017; Nguyen et al., 2021). Regarding dyes, MB in UV–Vis spectrum shows absorption peaks at 591 nm and 653 nm due to n → π* transition, whereas CR exhibits absorption peaks at 349 nm and 487 nm due to π → π* and n → π* azo group transitions. In MO UV–Vis spectrum, the absorption peak at 239 nm is due to the formation of amine group from MO dye degradation. $NaBH_4$, a strong reducing agent is incapable of reducing these dyes efficiently due to the large differences of redox potential, and hence, the reaction is thermally favourable but kinetically forbidden. Therefore, some catalyst is required to speed up the dyes reduction process. From results of the dyes UV–Vis spectra, it is inferred that the intensities of the prominent peaks are decreased with the passage of time and decolourization is completed after 180 min. Due to a large difference of reduction potential of dyes (acceptor) and $BH_4^-$ ions (donor), the transfer of electron between them via nanocatalysts becomes easy.

## 5. Conclusions

This study reports the synthesis of silver nanoparticles via aqueous extracts of *R. javanica, R. hastatus,* and *C. viminalis* plants. For the selected plants, well-dispersed, stable, and spherical RJAgNPs were produced in the ratios of 1:15 when kept at incubation, RHAgNPs in 1:16 under heating and stirring, and CVAgNPs in 1:9 when kept in sunlight. The subject AgNPs exhibited potential *in vitro* antioxidant activity against ABTS and antibacterial activity against *S. aureus*. In addition, the synthesized AgNPs significantly degraded the selected organic dyes, nitrophenols, and food colours. Conclusively, the subject AgNPs might be helpful in the free radical involving and infectious diseases as well as in the environmental remediation.

## Declaration of Competing Interest

The authors declare that they have no known competing financial interests or personal relationships that could have appeared to influence the work reported in this paper.

## Acknowledgement

The authors acknowledge the Higher Education Commission (HEC) for awarding a research grant (8967/KPK/NRPU/R&D/HEC/2017).

## Appendix A. Supplementary material

Supplementary data to this article can be found online at https://doi.org/10.1016/j.sjbs.2021.10.016.

## References

Ahmad, S., Ullah, F., Ayaz, M., Zeb, A., Ullah, F., Sadiq, A., 2016a. Antitumor and anti-angiogenic potentials of isolated crude saponins and various fractions of *Rumex hastatus* D. Don. Biol. Res. 49, 18. https://doi.org/10.1186/s40659-016-0079-2.

Ahmad, S., Ullah, F., Sadiq, A., Ayaz, M., Imran, M., Ali, I., Zeb, A., Ullah, F., Shah, M.R., 2016b. Chemical composition, antioxidant and anticholinesterase potentials of essential oil of *Rumex hastatus* D. Don collected from the North West of Pakistan. BMC Complement. Altern. Med. 16, 29. https://doi.org/10.1186/s12906-016-0998-z.

ElMitwalli, O.S., Barakat, O.A., Daoud, R.M., Akhtar, S., Henari, F.Z., 2020. Green synthesis of gold nanoparticles using cinnamon bark extract, characterization, and fluorescence activity in Au/eosin Y assemblies. J. Nanoparticle Res. 22, 309. https://doi.org/10.1007/s11051-020-04983-8.

Erci, F., Cakir-Koc, R., Isildak, I., 2018. Green synthesis of silver nanoparticles using *Thymbra spicata* L. var. *spicata* (zahter) aqueous leaf extract and evaluation of their morphology-dependent antibacterial and cytotoxic activity. Artif. Cells Nanomed. Biotechnol. 46 (sup1), 150–158. https://doi.org/10.1080/21691401.2017.1415917.

Ezhilarasu, H., Vishalli, D., Dheen, S.T., Bay, B.H., Srinivasan, D.K., 2020. Nanoparticle-based therapeutic approach for diabetic wound healing. Nanomaterials 10, 1234. https://doi.org/10.3390/nano10061234.

Farhadi, S., Ajerloo, B., Mohammadi, A., 2017. Green biosynthesis of spherical silver nanoparticles by using date palm (*Phoenix dactylifera*) fruit extract and study of their antibacterial and catalytic activities. Acta Chim. Slov. 64, 129–143.

Hassan, K.T., Ibraheem, I.J., Hassan, O.M., Obaid, A.S., Ali, H.H., Salih, T.A., Kadhim, M. S., 2021. Facile green synthesis of Ag/AgCl nanoparticles derived from Chara algae extract and evaluating their antibacterial activity and synergistic effect with antibiotics. J. Environ. Chem. Eng. 9 (4), 105359. https://doi.org/10.1016/j.jece:2021.105359.

Jadhav, S.A., Garud, H.B., Patil, A.H., Patil, G.D., Patil, C.R., Dongale, T.D., Patil, P.S., 2019. Recent advancements in silica nanoparticles based technologies for removal of dyes from water. Colloids Interface Sci. Commun. 30,. https://doi.org/10.1016/j.colcom.2019.100181 100181.

Jadoun, S., Arif, R., Jangid, N.K., Meena, R.K., 2021. Green synthesis of nanoparticles using plant extracts: A review. Environ. Chem. Lett. 19, 355–374. https://doi.org/10.1007/s10311-020-01074-x.

Jain, S., Mehata, M.S., 2017. Medicinal plant leaf extract and pure flavonoid mediated green synthesis of silver nanoparticles and their enhanced antibacterial property. Sci. Rep. 7, 15867. https://doi.org/10.1038/s41598-017-15724-8.

Jamila, N., Khairuddean, M., Yaacob, N.S., Kamal, N.N.S.N.M., Osman, H., Khan, S.N., Khan, N., 2014. Cytotoxic benzophenone and triterpene from *Garcinia hombroniana*. Bioorg. Chem. 54, 60–67. https://doi.org/10.1016/j.bioorg.2014.04.003.

Jamila, N., Khan, N., Bibi, A., Haider, A., Noor Khan, S., Atlas, A., Nishan, U., Minhaz, A., Javed, F., Bibi, A., 2020. *Piper longum* catkin extract mediated synthesis of Ag, Cu, and Ni nanoparticles and their applications as biological and environmental remediation agents. Arab. J. Chem. 13 (8), 6425–6436. https://doi.org/10.1016/j.arabjc.2020.06.001.

Jamila, N., Khan, N., Bibi, N., Waqas, M., Khan, S.N., Atlas, A., Amin, F., Khan, F., Saba, M., 2021. Hg (II) sensing, catalytic, antioxidant, antimicrobial, and anticancer potential of *Garcinia mangostana* and α-mangostin mediated silver nanoparticles. Chemosphere 272, 129794. https://doi.org/10.1016/j.chemosphere.2021.129794.

Kamnev, A.A., Dyatlova, Y.A., Kenzhegulov, O.A., Vladimirova, A.A., Mamchenkova, P. V., Tugarova, A.V., 2021. Fourier Transform Infrared (FTIR) Spectroscopic analyses of microbiological samples and biogenic selenium nanoparticles of microbial origin: sample preparation effects. Molecules 26, 1146. https://doi.org/10.3390/molecules26041146.

Kim, K.J., Kim, Y.H., Yu, H.H., Jeong, S.I., Cha, J.D., Kil, B.S., You, Y.O., 2003. Antibacterial activity and chemical composition of essential oil of Chrysanthemum boreale. Planta Med. 69, 274–277. https://doi.org/10.1055/s-2003-38479.

Khan, Z.U.H., Khan, A., Chen, Y., Khan, U.A., Shah, N.S., Muhammad, N., Murtaza, B., Tahir, K., Khan, F.U., Wan, P., 2017. Photo catalytic applications of gold nanoparticles synthesized by green route and electrochemical degradation of phenolic Azo dyes using AuNPs/GC as modified paste electrode. J. Alloys Compd. 725, 869–876. https://doi.org/10.1016/j.jallcom.2017.07.222.

Khan, S.A., Khan, S.B., Farooq, A., Asiri, A.M., 2019. A facile synthesis of CuAg nanoparticles on highly porous ZnO/carbon black-cellulose acetate sheets for nitroarene and azo dyes reduction/degradation. Int. J. Biol. Macromol. 130, 288–299. https://doi.org/10.1016/j.ijbiomac.2019.02.114.

Liang, H.-X., Dai, H.-Q., Fu, H.-A., Dong, X.-P., Adebayo, A.H., Zhang, L.-X., Cheng, Y.-X., 2010. Bioactive compounds from *Rumex* plants. Phytochem. Lett. 3 (4), 181–184. https://doi.org/10.1016/j.phytol.2010.05.005.

Lin, N., Verma, D., Saini, N., Arbi, R., Munir, M., Jovic, M., Turak, A., 2021. Antiviral nanoparticles for sanitizing surfaces: a roadmap to self-sterilizing against COVID-19. Nano Today 40, 101267. https://doi.org/10.1016/j.nantod.2021.101267.

Liu, H.-X., Chen, Y.-C., Liu, Y., Zhang, W.-M., Wu, J.-W., Tan, H.-B., Qiu, S.-X., 2016. Acylphloroglucinols from the leaves of *Callistemon viminalis*. Fitoterapia 114, 40–44. https://doi.org/10.1016/j.fitote.2016.08.010.

Liu, H.-X., Tan, H.-B., Li, S.-N., Chen, Y.-C., Li, H.-H., Qiu, S.-X., Zhang, W.-M., 2018. Two new 12-membered macrolides from the endophytic fungal strain *Cladosprium colocasiae* A801 of *Callistemon viminalis*. J. Asian Nat. Prod. Res. 21, 696-701. https://doi.org/10.1080/10286020.2018.1471067.

Loo, Y.Y., Rukayadi, Y., Nor-Khaizura, M.A.R., Kuan, C.H., Chieng, B.W., Nishibuchi, M., Radu, S., 2018. *In vitro* antimicrobial activity of green synthesized silver nanoparticles against selected gram-negative foodborne pathogens. Front Microbiol. 9, 1555.

Makkar, H.P.S., Singh, B., Vats, S.K., Sood, R.P., 1993. Total phenols, tannins and condensed tannins in different parts of *Rumex hastatus*. Bioresour. Technol. 45 (1), 69–71. https://doi.org/10.1016/0960-8524(93)90147-4.

Marslin, G., Siram, K., Maqbool, Q., Selvakesavan, R.K., Kruszka, D., Kachlicki, P., Franklin, G., 2018. Secondary metabolites in the green synthesis of metallic nanoparticles. Materials 11, 940. https://doi.org/10.3390/ma11060940.

Mishra, A. P., Sharifi-Rad, M., Shariati, M. A., Mabkhot, Y. N., Al-Showiman, S. S., Rauf, A., Salehi, B., Župunski, M., Sharifi-Rad, M., Gusain, P., 2018. Bioactive compounds and health benefits of edible *Rumex* species-A review. Cell. Mol. Biol. 64, 27–34. https://doi.org/10.14715/cmb/2018.64.8.5.

Nguyen, D.T.C., Le, H.T.N., Nguyen, T.T., Nguyen, T.T.T., Bach, L.G., Nguyen, T.D., Tran, T.V., 2021. Multifunctional ZnO nanoparticles bio-fabricated from *Canna indica* L. flowers for seed germination, adsorption, and photocatalytic degradation of organic dyes. J. Hazard. Mater 420, 126586. https://doi.org/10.1016/j.jhazmat.2021.126586.

Nobahar, A., Carlier, J.D., Miguel, M.G., Costa, M.C., 2021. A review of plant metabolites with metal interaction capacity: a green approach for industrial applications. BioMetals 34 (4), 761–793. https://doi.org/10.1007/s10534-021-00315-y.

Ouyang, M.-A., Wein, Y.-S., Zhang, Z.-K., Kuo, Y.-H., 2007. Inhibitory activity against tobacco mosaic virus (TMV) replication of pinoresinol and syringaresinol lignans and their glycosides from the root of *Rhus javanica* var. roxburghiana. J. Agric. Food Chem. 55 (16), 6460–6465. https://doi.org/10.1021/jf070980810.1021/jf0709808.s001.

Oyedeji, O.O., Lawal, O., Shode, F., Oyedeji, A., 2009. Chemical composition and antibacterial activity of the essential oils of *Callistemon citrinus* and *Callistemon viminalis* from South Africa. Molecules 14, 1990–1998. https://doi.org/10.3390/molecules14061990.

Sahreen, S., Khan, M.R., Khan, R.A., 2014. Comprehensive assessment of phenolics and antiradical potential of *Rumex hastatus* D. Don. roots. BMC Complement. Altern. Med. 14, 47. https://doi.org/10.1186/1472-6882-14-47.

Sahu, T., Ratre, Y.K., Chauhan, S., Bhaskar, L.V.K.S., Nair, M.P., Verma, H.K., 2021. Nanotechnology based drug delivery system: Current strategies and emerging therapeutic potential for medical science. J. Drug Deliv. Sci. Technol. 63, 102487. https://doi.org/10.1016/j.jddst.2021.102487.

Salem, M.ZM., Ali, H.M., El-Shanhorey, N.A., Abdel-Megeed, A., 2013. Evaluation of extracts and essential oil from *Callistemon viminalis* leaves: Antibacterial and antioxidant activities, total phenolic and flavonoid contents. Asian Pac. J. Trop. Med. 6 (10), 785–791. https://doi.org/10.1016/S1995-7645(13)60139-X.

Salem, M.Z., Mervat, E.-H., Nasser, R.A., Ali, H.M., El-Shanhorey, N.A., Elansary, H.O., 2017. Medicinal and biological values of *Callistemon viminalis* extracts: History, current situation and prospects. Asian Pac. J. Trop. Med. 10, 229–237. https://doi.org/10.1016/j.apjtm.2017.03.015.

Soni, V., Raizada, P., Singh, P., Cuong, H.N., Rangabhashiyam, S., Saini, A., Saini, R.V., Van Le, Q., Nadda, A.K., Le, T.-T., 2021. Sustainable and green trends in using plant extracts for the synthesis of biogenic metal nanoparticles toward

environmental and pharmaceutical advances: A review. Environ. Res. 111622. https://doi.org/10.1016/j.envres.2021.111622.
Wu, W., Kong, X., Zhang, C., Hua, Y., Chen, Y., 2018. Improving the stability of wheat gliadin nanoparticles–Effect of gum arabic addition. Food hydrocoll. 80, 78–87. https://doi.org/10.1016/j.foodhyd.2018.01.042.
Yang, D., Fan, R., Luo, F., Chen, Z., Gerson, A.R., 2021. Facile and green fabrication of efficient Au nanoparticles catalysts using plant extract via a mesoporous silica-assisted strategy. Colloids Surf. A: Physicochem. Eng. Asp. 621, 126580. https://doi.org/10.1016/j.colsurfa.2021.126580.
Yu, C., Schimelman, J., Wang, P., Miller, K.L., Ma, X., You, S., Guan, J., Sun, B., Zhu, W., Chen, S., 2020. Photopolymerizable biomaterials and light-based 3D printing strategies for biomedical applications. Chem. Rev. 120, 10695–10743. https://doi.org/10.1021/acs.chemrev.9b00810.